Membrane tethering by the atlastin GTPase depends on GTP hydrolysis but not on forming the cross-over configuration

Simran G. Saini[a], Chuang Liu[b], Peijun Zhang[b], and Tina H. Lee[a]
[a]Department of Biological Sciences, Carnegie Mellon University, Pittsburgh, PA 15213; [b]Department of Structural Biology, University of Pittsburgh, Pittsburgh, PA 15260

ABSTRACT **The membrane-anchored atlastin GTPase couples nucleotide hydrolysis to the catalysis of homotypic membrane fusion to form a branched endoplasmic reticulum network. *Trans* dimerization between atlastins anchored in opposing membranes, accompanied by a cross-over conformational change, is thought to draw the membranes together for fusion. Previous studies on the conformational coupling of atlastin to its GTP hydrolysis cycle have been carried out largely on atlastins lacking a membrane anchor. Consequently, whether fusion involves a discrete tethering step and, if so, the potential role of GTP hydrolysis and cross-over in tethering remain unknown. In this study, we used membrane-anchored atlastins in assays that separate tethering from fusion to dissect the requirements for each. We found that tethering depended on GTP hydrolysis, but, unlike fusion, it did not depend on cross-over. Thus GTP hydrolysis initiates stable head-domain contact in *trans* to tether opposing membranes, whereas cross-over formation plays a more pivotal role in powering the lipid rearrangements for fusion.**

Monitoring Editor
Benjamin S. Glick
University of Chicago

Received: Aug 15, 2014
Revised: Sep 15, 2014
Accepted: Sep 16, 2014

INTRODUCTION

Atlastin (ATL) is a large membrane-anchored GTPase required to form the branched endoplasmic reticulum (ER) network in organisms ranging from yeast to human (Park and Blackstone, 2010; McNew *et al.*, 2013). The requirement for ATL in ER network formation may reflect its role in one or more membrane-shaping processes, including membrane curvature, tubule extension, and/or membrane fusion (Lee and Chen, 1988; Lee *et al.*, 1989; Allan and Vale, 1991; Waterman-Storer, 1998; Friedman *et al.*, 2010; Shibata *et al.*, 2010). However, the remarkable finding that *Drosophila melanogaster* ATL (D-ATL), as well as the distantly related yeast SEY1 and *Arabidopsis* RHD3 orthologues, can catalyze GTP-dependent fusion when purified and inserted into synthetic liposomes is most consistent with a direct role for ATL in homotypic membrane fusion (Orso *et al.*, 2009; Anwar *et al.*, 2012; Zhang *et al.*, 2013).

Current models for the ATL fusion mechanism are based on several key findings. First, fusion depends strictly on GTP hydrolysis. The nonhydrolyzable GTP analogue guanosine 5-*O*-[gamma-thio] triphosphate (GTPγS) failed to substitute for GTP (Orso *et al.*, 2009; Moss *et al.*, 2011), and the hydrolysis-defective R48A D-ATL variant failed to catalyze fusion even when GTP was provided (Pendin *et al.*, 2011; Byrnes *et al.*, 2013). Second, x-ray crystal structure determinations of the ATL1 soluble domain initially revealed two distinct dimer configurations (Bian *et al.*, 2011; Byrnes and Sondermann, 2011). Both configurations had the GTPases interacting in a head-to-head manner with bound nucleotides near the dimer interface. However, the conformers also differed from one another markedly. In one (form 2), the three-helix bundle (3HB) comprising the middle domain of each subunit was bent back away from the dimer interface axis, packing against a helix (α6) within the GTPase head of the same subunit (Bian *et al.*, 2011; Byrnes and Sondermann, 2011). By contrast, the other conformer (form 1) lacked the intramolecular 3HB-head interactions observed in the form 2 conformer, due to the release of the 3HB from the head and a subsequent rigid body rotation about a conserved proline within the linker connecting the 3HB to the head. The rotation of the 3HB causes the middle domains to cross over one another, bringing the 3HBs, pointing away from one

This article was published online ahead of print in MBoC in Press (http://www.molbiolcell.org/cgi/doi/10.1091/mbc.E14-08-1284) on September 24, 2014.
Address correspondence to: Tina H. Lee (thl@andrew.cmu.edu).
Abbreviations used: 3HB, three-helix bundle; ATL, atlastin; cryo-EM, cryo-electron microscopy; D-ATL, *Drosophila melanogaster* atlastin; DLS, dynamic light scattering; ER, endoplasmic reticulum; FL, full length; GTPγS, 5-*O*-[gamma-thio] triphosphate; RT, room temperature; TM, transmembrane.

another initially in an extended configuration, into close parallel alignment (Bian *et al.*, 2011; Byrnes and Sondermann, 2011; Byrnes *et al.*, 2013). Additionally, cross-over buries a much larger surface area (>3.5-fold) between subunits, creating a more stable configuration (Bian *et al.*, 2011; Byrnes and Sondermann, 2011; Byrnes *et al.*, 2013).

In addition to conformational changes within the GTPase and 3HB domains, a requirement for the cytoplasmic tail of ATL was also demonstrated (Moss *et al.*, 2011; Liu *et al.*, 2012). Though the tail primary sequence is not well conserved, it is characterized by a predicted amphipathic helix just proximal to the second membrane-spanning segment. A peptide derived from this helix in D-ATL penetrated into the lipid bilayer, and this ability correlated with fusion activity in vitro (Liu *et al.*, 2012). Thus tail insertion was proposed to contribute a key lipid-destabilizing force necessary for fusion.

Based on the above findings, a consensus model for the ATL mechanism has emerged: GTP binding and hydrolysis, with help from the C-terminal tail, drives fusion by drawing opposing membrane-anchored ATL soluble domains together in *trans* and inducing cross-over formation. Yet there is still little agreement on the details of the fusion mechanism. At first, the lack of consensus was attributed to the uncertainty of the nucleotide-bound state for each of the initial crystal structure dimer conformers. Irrespective of the nucleotide analogue used during crystallization, only GDP was observed in the active site (Bian *et al.*, 2011; Byrnes and Sondermann, 2011). Despite this, dimers were suggested to form in the GTP-bound state independent of nucleotide hydrolysis, because stable dimers were recovered after incubation with the nonhydrolyzable GTP analogue GMPPNP, even though they were also recovered with the transition-state analogue GDP-AlF_4^- (Byrnes and Sondermann, 2011; Morin-Leisk *et al.*, 2011; Moss *et al.*, 2011). Subsequent chemical cross-linking and cryo-electron microscopy (cryo-EM) analysis revealed that the GMPPNP dimers were in the cross-over configuration (Morin-Leisk *et al.*, 2011). This observation was confirmed by more recent x-ray crystal structure determinations revealing an additional form 3 cross-over dimer conformer resembling the previously observed form 1 conformer, though with clear differences in the active site and also exhibiting more tightly packed interactions overall (Byrnes *et al.*, 2013). The form 3 dimer, produced upon crystallization with either GMPPNP or GDP-AlF_4^-, retained the respective analogues in the active site, indicating that ATL1 is capable of adopting the tightly packed cross-over configuration in at least two distinct nucleotide-bound states. Collectively the observations failed to resolve whether dimer formation and/or cross-over require nucleotide hydrolysis.

Fortunately, recent kinetic measurements revealed that both dimer formation and cross-over, at least in the soluble phase, are catalyzed by nucleotide hydrolysis. Using FRET-based probes to independently monitor head-to-head contact and cross-over formation within the truncated ATL1 soluble domain, Sondermann and colleagues observed relatively efficient head contact and cross-over with GMPPNP, as predicted from earlier studies. Remarkably, however, both head contact and cross-over were accelerated two orders of magnitude (from $t_{1/2}$ ~100 s to $t_{1/2}$ ~1 s) in the presence of hydrolyzable GTP (Byrnes *et al.*, 2013).

Of significance, previous studies probing the conformational coupling of ATL to its GTP hydrolysis cycle have largely been carried out in the soluble phase, using molecules lacking a membrane anchor (Bian *et al.*, 2011; Byrnes and Sondermann, 2011; Byrnes *et al.*, 2013; Morin-Leisk *et al.*, 2011; Moss *et al.*, 2011). This might present a serious caveat if the soluble domain were to behave differently from its membrane-anchored counterpart, possibly due to greater flexibility in the absence of membrane anchoring. To address this issue, we used membrane-anchored ATL to analyze the requirement for both GTP hydrolysis and for cross-over in the context of both membrane tethering and membrane fusion reactions. Similar to the recent model put forth by Sondermann and colleagues, in which energy input is required at the earliest *trans* pairing step of the fusion reaction (Byrnes *et al.*, 2013), our results revealed a clear requirement for nucleotide hydrolysis in the stable *trans* pairing of ATL molecules during vesicle tethering. However, unlike the recently proposed model, our findings also revealed that cross-over can be uncoupled from tethering by mutation. Thus cross-over formation, though possibly catalyzed in concert with tethering by nucleotide hydrolysis as put forth recently (Byrnes *et al.*, 2013), nevertheless plays a more pivotal role in driving membrane fusion than in membrane tethering.

RESULTS

Membrane-tethering assay

To clarify the energetics of *trans* dimer formation in the context of membranes, we set out to establish an assay that would independently evaluate the requirements for ATL-mediated membrane tethering, apart from fusion. For the tethering assay, we wanted to adhere closely to fusion conditions to maximize the relevance of our findings. However, because fusion could complicate the evaluation of tethering, we expressly prevented fusion, at least at the outset, by using membrane-anchored versions of ATL with small C-terminal truncations removing the cytoplasmic tail and/or the second transmembrane (TM) helix. Truncation had previously been reported to block fusion (Moss *et al.*, 2011; Liu *et al.*, 2012), but we reasoned that it might not adversely impact tethering, because *trans* interactions between TM helices or the tail had not been reported. Furthermore, because human ATL had not yet been reported to catalyze fusion, we used D-ATL, which catalyzes fusion robustly in a GTP hydrolysis–dependent manner and is ~50% identical to ATL1/2/3 (Orso *et al.*, 2009; Bian *et al.*, 2011). To first confirm that the truncated constructs were fusion incompetent under our assay conditions, we assessed their fusion kinetics relative to the full-length (FL) protein. As expected, fusion by FL D-ATL was strictly dependent on GTP hydrolysis, with no fusion signal either in the absence of nucleotide or in the presence of GMPPNP (Figure 1). Also as anticipated (Moss *et al.*, 2011; Liu *et al.*, 2012), both the tailless protein and a further truncated protein, containing just the first TM helix (single TM D-ATL; Liu *et al.*, 2012), were entirely defective for fusion (Figure 1).

Membrane tethering assessed by dynamic light scattering

On the basis of our expectation that tethering of individual proteoliposomes in the absence of fusion should generate larger proteoliposome clusters, we used dynamic light scattering (DLS), which is well-suited to detecting such size changes (Arac *et al.*, 2006). Proteoliposomes for the tethering assay were prepared in the same manner as for the fusion assay. Single TM D-ATL proteoliposomes, confirmed to be fusion incompetent (Figure 1), were incubated with GTP-Mg^{+2} at 37°C for varying times, and the mean hydrodynamic diameters of both the starting and resulting liposome populations were monitored. The starting proteoliposomes were relatively monodisperse with a 200- to 300-nm mean hydrodynamic diameter (*z*-average; Supplemental Figure S1 and Figure 2A). On addition of GTP-Mg^{+2}, the samples became polydisperse and the *z*-average increased rapidly, reaching values on the order of several microns by 10 min (Figure 2A). The observed size shift was temperature dependent and reversed by EDTA treatment, consistent with GTP-Mg^{+2} dependence (Figure 2B). Notably, even without EDTA

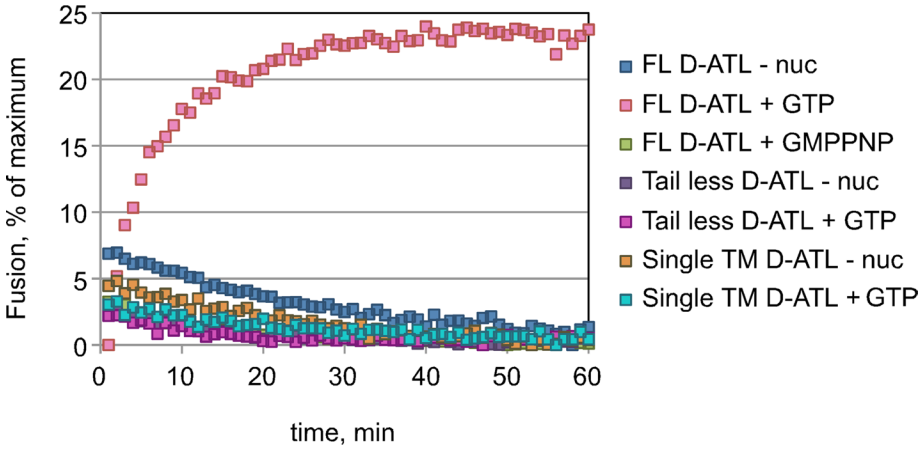

FIGURE 1: Tailless and single TM D-ATL are fusion incompetent. FL, tailless (residues 1–471), or single TM (residues 1–447) D-ATL was reconstituted into donor and acceptor vesicles. Fusion was monitored by the dequenching of NBD-labeled lipid present in the donor vesicles after addition of GTP or GMPPNP or in the absence of nucleotide.

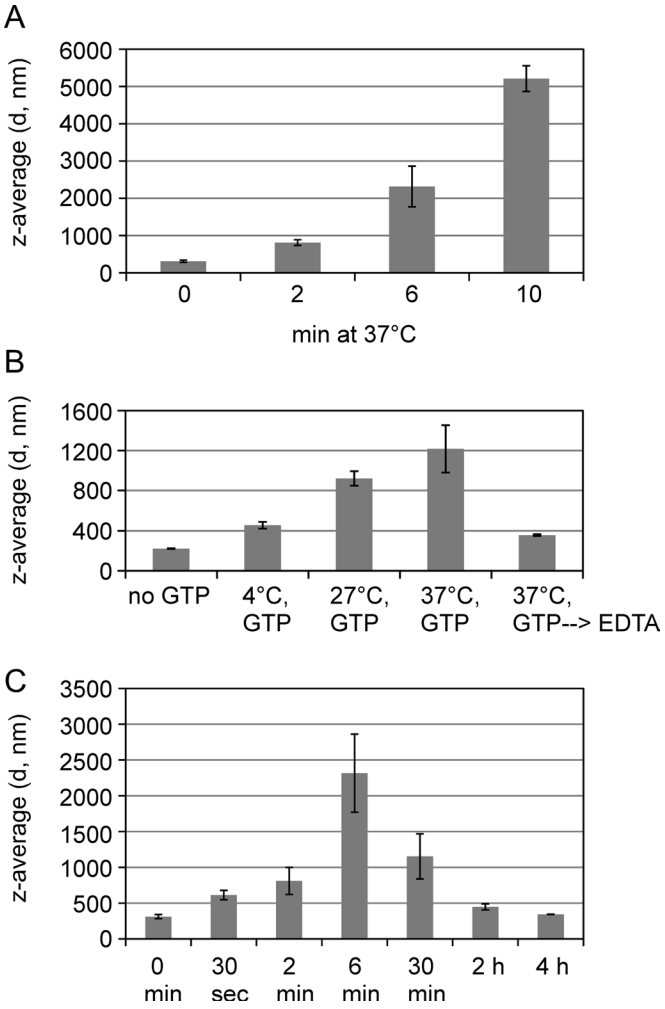

FIGURE 2: Fusion-incompetent D-ATL is capable of tethering membranes. (A) Tethering is time dependent. Single TM D-ATL was reconstituted into vesicles and incubated with GTP at 37°C for the indicated times before DLS measurements. (B) Tethering is temperature dependent. Vesicles were incubated at the indicated temperatures in the absence of GTP (37°C) or presence of GTP at the indicated temperatures for 10 min; this was followed by DLS. The 37°C GTP samples were further treated with EDTA and remeasured by DLS. (C) Tethering is reversible. Prolonged incubation at 37°C led to reversal of tethering as indicated by DLS. In each case, the average of three independent measurements ± SD is shown.

treatment, the GTP-Mg^{+2}–induced size shift was reversed after prolonged incubation, driven possibly by dimer disassembly after GTP depletion (Figure 2C; Morin-Leisk *et al.*, 2011; Byrnes *et al.*, 2013).

GTP-dependent membrane tethering visualized by cryo-EM

To complement the DLS assay, we also performed cryo-EM analysis, which revealed the morphology of a putative GTP-dependent ATL-tethered intermediate (Figure 3). After brief incubation with or without GTP, samples were deposited onto EM grids and immediately subjected to plunge freezing. Overview images taken at low magnification showed large clusters of vesicles in the GTP sample, often 1 to 2 µm in length, compared with a more dispersed arrangement in the absence of GTP (Figure 3A). D-ATL–mediated vesicle tethering was directly visualized as zipper-like parallel-aligned membrane interfaces within each cluster in the GTP sample (Figure 3B, with a further enlarged image shown in Figure 3C, left panel). These structures were likely formed through extended interactions between single TM D-ATL in opposing proteoliposomes. Importantly, the zipper-like structures were seen more frequently with GTP than without, consistent with the DLS results (Figure 3D, WT, black vs. gray bars).

Tethering depends on GTP hydrolysis

Next we assessed the dependence of tethering on GTP hydrolysis. The nonhydrolyzable analogue GMPPNP was used, because it promoted stable dimer formation of the truncated ATL1/2 soluble domain (Byrnes and Sondermann, 2011; Byrnes *et al.*, 2013; Morin-Leisk *et al.*, 2011), albeit more slowly than GTP (Byrnes *et al.*, 2013). Moreover, the form 3 ATL1 dimer structure was crystallized with GMPPNP and clearly retained the analogue within the active site (Byrnes *et al.*, 2013). Based on prior soluble-phase data, including our own (Morin-Leisk *et al.*, 2011), our expectation was that tethering would occur readily with GMPPNP but possibly more slowly than with GTP. Strikingly, there was robust tethering of single TM D-ATL proteoliposomes only in the presence of GTP. Neither GDP nor GMPPNP could promote it, indicating a strict dependence on nucleotide hydrolysis (Figure 4). Similar results were obtained using a version of D-ATL lacking the tail but retaining the second TM helix (Figure 4). Additionally, another nonhydrolyzable analogue (GTPγS) also failed to support tethering (Supplemental Figure S2).

We were struck by the apparent lack of tethering in the absence of nucleotide hydrolysis. Unfortunately, AlF_4^- by itself caused membranes to aggregate, rendering a test of the transition-state analogue GDP-AlF_4^- unfeasible in this assay. Instead, we sought an independent means of confirming the nucleotide hydrolysis requirement. For this, we took advantage of D-ATL variants with mutations in a key conserved catalytic residue R48, which when mutated to R48E or R48A, abolishes GTPase activity (Bian *et al.*, 2011; Byrnes and Sondermann, 2011; Pendin *et al.*, 2011). In the form 3

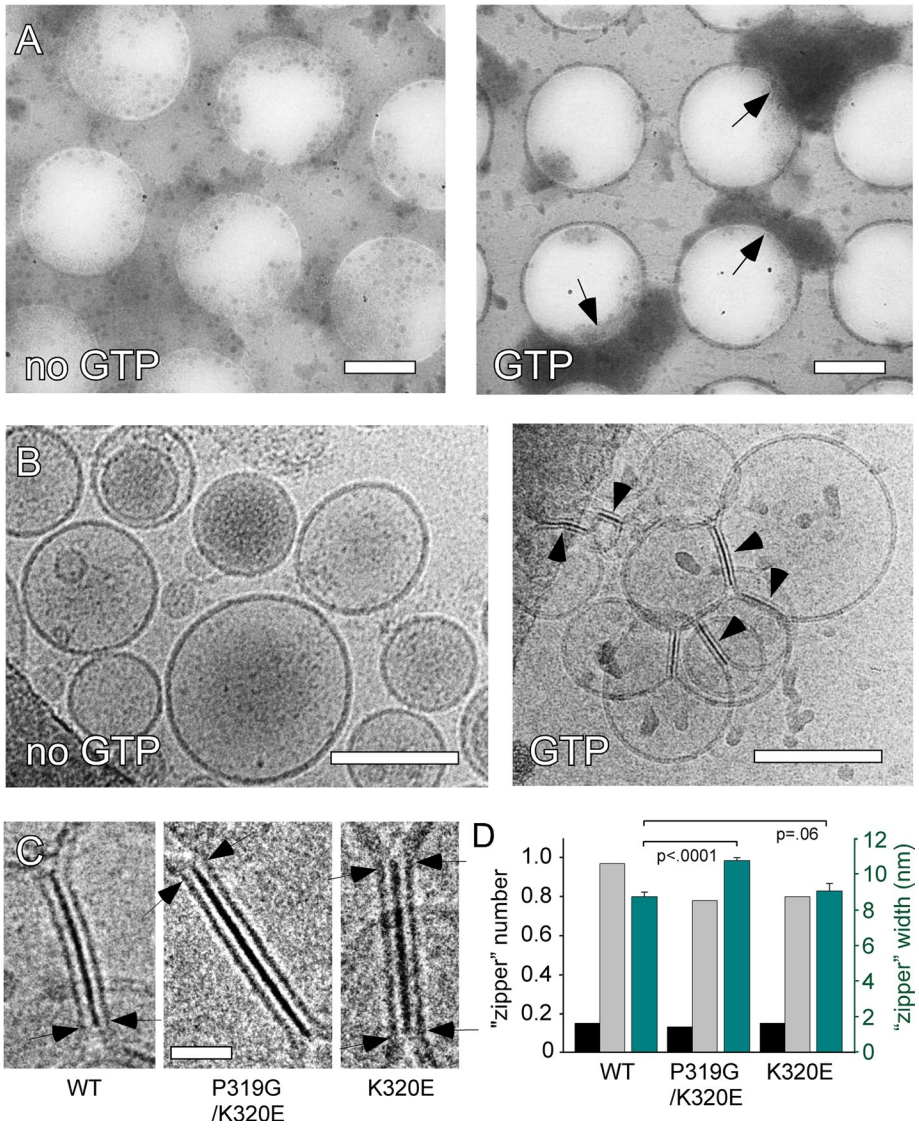

FIGURE 3: Cryo-EM visualization of vesicle tethering by D-ATL. (A and B) Single TM D-ATL reconstituted into vesicles was incubated at RT for 20 min in the absence or presence of GTP and imaged with cryo-EM at low (A) and high (B) magnification. Scale bars: (A) 1 μm; (B) 100 nm. Arrowheads (B) mark zipper-like structures formed between opposing membranes. (C) Enlarged views of the zipper-like structures from wild-type single TM (left), P319G K320E FL (middle), and K320E FL (right) D-ATL. Arrows indicate where two membranes are "zippered" together. Scale bar: 20 nm. (D) Comparison of the average number of tethered structures per micrograph, in the absence (black) and presence (gray) of GTP. Data shown are from 70–100 micrographs per sample. Also shown is a comparison of the average width of the "zippers" (green) in the presence of GTP from wild-type single TM, P319G K320E FL and K320E FL D-ATL samples. Measurements are derived from >10 "zippers" for each, ± SD The indicated *p* values were determined using an unpaired Student's *t* test.

dimer conformer, the R48 side chain was observed to point in toward each respective active site, functioning as an intramolecular arginine finger to stabilize the negatively charged hydrolytic transition state (Byrnes *et al.*, 2013). However, in the form 1 and 2 dimer conformers, the same side chain was observed to point out toward the dimer interface (Bian *et al.*, 2011; Byrnes and Sondermann, 2011). Thus R48 may swing away from the dimer interface en route to hydrolysis, moving in toward the active site to perform its catalytic function. A similar dimer-dependent rearrangement of the same R48 catalytic residue occurs in the closely related human guanylate-binding protein 1 (Ghosh *et al.*, 2006). Accordingly, charge reversal to R48E (R77E in ATL1) blocked GTP hydrolysis as well as stable dimer formation with either GMPPNP or GDP-AlF_4^-, presumably by introducing charge repulsion at the dimer interface (Byrnes and Sondermann, 2011). In contrast, charge removal to alanine (R48A) did not impair GMPPNP-dependent stable dimer formation in the soluble phase, likely because the remaining head contacts were sufficient for dimerization (Pendin *et al.*, 2011; Byrnes *et al.*, 2013). However, elimination of the positive charge within the active site, normally provided by the arginine finger, nearly eliminated hydrolytic activity (Pendin *et al.*, 2011; Byrnes *et al.*, 2013). Confirming our results with GMPPNP (Figure 4) and GTPγS (Supplemental Figure S2), neither the R48A nor R48E variant was capable of tethering vesicles (Figure 4). It is worth mentioning that ATL is consistently monomeric in the absence of nucleotide or in the presence of GDP (Byrnes and Sondermann, 2011; Morin-Leisk *et al.*, 2011; Moss *et al.*, 2011), and because our membrane-anchored D-ATL was prepared in the absence of nucleotide, it was unlikely that hydrolysis was serving to break up preexisting ATL cross-over dimers. Altogether these results established, for the first time, that tethering by membrane-anchored D-ATL requires energy input from GTP hydrolysis. Notably, the lack of any detectable vesicle tethering with GMPPNP contrasted with previously observed formation of GMPPNP-induced stable, truncated, soluble-domain dimers (Byrnes and Sondermann, 2011; Morin-Leisk *et al.*, 2011). The difference, though it remains to be demonstrated, may reflect further slowing of hydrolysis-independent cross-over (observed with truncated ATL) by the conformational constraints imposed by membrane anchoring.

Tethering does not depend on a salt bridge required for fusion

On the basis of the hydrolysis requirement for tethering (Figure 4) combined with the prior observation that hydrolysis catalyzed concerted head contact and cross-over in the soluble phase (Byrnes *et al.*, 2013), we anticipated that cross-over formation would also be required for tethering (Byrnes *et al.*, 2013). Work from our lab had previously shown that the cross-over dimer configuration of soluble ATL2 depends on an intramolecular salt bridge between two oppositely charged residues at the heart of the cross-over in the ATL1 crystal structures (Morin-Leisk *et al.*, 2011). One residue, K372, is in the linker connecting the GTPase head to the 3HB; and the other residue, E380, is nearby at the start of the 3HB (Figure 5A). Though the K372-E380 salt bridge is intramolecular, it likely stabilizes a kinked conformation of the linker in each monomer; the kink in turn promotes cross-over dimer formation by facilitating intermolecular packing interactions. Supporting this hypothesis, charge reversal of

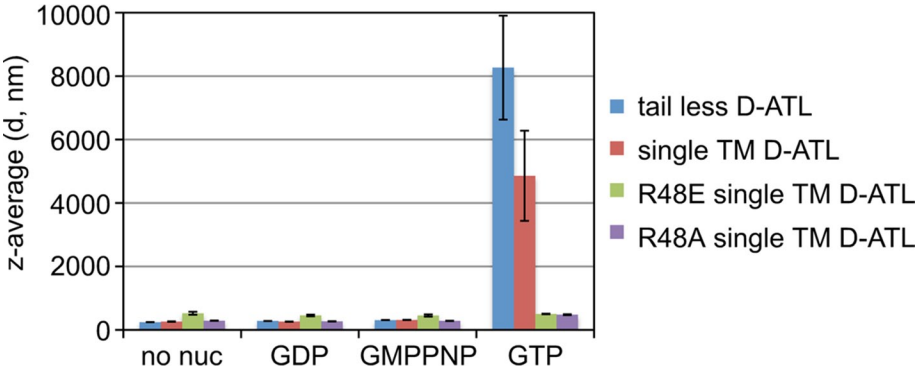

FIGURE 4: Tethering depends on GTP hydrolysis. Wild-type, R48E (both dimerization incompetent and hydrolysis defective), or R48A (dimerization competent but hydrolysis defective) mutant variants of single TM D-ATL were reconstituted into vesicles and incubated at 37°C for 10 min in the presence or absence of the indicated nucleotides and subjected to DLS. A tailless version of wild-type D-ATL is also shown. The average of three independent measurements ± SD is shown for each condition

either of the residues (K372E or E380R) impaired formation of a cross-linked product predicted to depend on cross-over (Morin-Leisk *et al.*, 2011). These mutations also had functional consequences, blocking the ability of ATL2 to support ER network formation in cells (Morin-Leisk *et al.*, 2011). Attesting to the specificity of the charge-reversal mutations, the inhibitory effects of each single charge-reversal mutation were fully rescued in the compensatory double mutant (K372E,E380R; Morin-Leisk *et al.*, 2011). Of relevance to this work, K372 and E380 are conserved not only between ATL1 and ATL2, but also in D-ATL. Moreover, charge reversal of either of the corresponding residues in D-ATL (K320E and E328R) had previously been reported to block fusion (Bian *et al.*, 2011). Consequently we reasoned that the corresponding salt bridge in D-ATL would be essential for fusion and that mutations perturbing it might prove useful for testing the dependence of membrane tethering on cross-over.

To assess whether K320 and E328 form a required salt bridge for D-ATL, we first expressed each charge-reversal mutation in the context of FL D-ATL. Like ATL2, wild-type D-ATL expression did not adversely affect the branched ER network morphology in Cos-7 cells (Figure 5B, quantified in 5C). In contrast, and as previously observed for ATL2 (Morin-Leisk *et al.*, 2011), expression of either the K320E or E328R D-ATL variant led to dominant-negative perturbations of the ER, including loss of the tubular network in the periphery and collapse into bundles or aggregates of ER membrane (Figure 5B, quantified in 5C). Although the perturbations were stronger for K320E than for E328R (Figure 5C), the dominant-negative effects of either mutation were fully rescued in the double-mutant variant (Figure 5B, quantified in 5C), again attesting to the importance of the salt bridge for in vivo functionality. Up to this point, the analogous mutations in D-ATL seemed to behave similarly to those in ATL2, consistent with conservation of the salt bridge as a stabilizing force for forming the cross-over dimer. That these and other D-ATL variants were correctly ER targeted was confirmed by counterstaining for cotransfected REEP5, a tubular ER marker (Hashimoto *et al.*, 2014; Supplemental Figure S3).

For confirming the importance of the K320-E328 salt bridge for fusion, both single- and double-mutant variants were constructed in the context of FL D-ATL and incorporated into liposomes for the fusion assay. Neither the K320E nor the E328R variant had fusion activity, as anticipated (Figure 5D; Bian *et al.*, 2011). Remarkably, the double-mutant variant catalyzed fusion to a similar extent as wild-type, though with slowed kinetics (Figure 5D). This result confirmed the importance of the K320-E328 salt bridge for fusion. Whether the compensatory mutation restored full lipid bilayer fusion, rather than selectively restoring outer leaflet mixing, remains to be determined, requiring additional assays that measure inner leaflet and content mixing (Orso *et al.*, 2009; Liu *et al.*, 2012).

Having established the importance of the K320-E328 salt bridge for fusion, we asked whether tethering would also depend on the salt bridge. The single TM D-ATL variants containing either the K320E or E328R mutation were assessed for tethering by DLS. To our surprise, both variants tethered membranes robustly and in a manner that depended on hydrolyzable GTP, contrasting with the nucleotide binding–defective R48E variant, which failed to tether under any condition (Figure 5E). Similar results were obtained with FL versions of the K320E and E328R mutant variants retaining the second TM helix and tail (Figure 5E). Thus, although membrane fusion depended considerably on the K320-E328 salt bridge, tethering did not.

Disruption of the D-ATL K320-E328 salt bridge does not abolish cross-over

Our results thus far suggested that tethering might be cross-over independent. Notably, though, our earlier work demonstrating the dependence of cross-over on the identified salt bridge had been carried out exclusively on ATL2. Consequently we needed to confirm the effect of the corresponding mutations on D-ATL cross-over. We therefore subjected the K320E variant of the D-ATL soluble domain to the same cross-linking analysis used previously to monitor ATL2 cross-over (Morin-Leisk *et al.*, 2011).

The 8-Å homobifunctional sulfhydryl cross-linker BMOE, is ideal for capturing ATL2 cross-over dimers, because two sulfhydryl 3HB residues (C395) come to within ~8 Å of one another uniquely in the cross-over dimer configuration (Bian *et al.*, 2011; Byrnes and Sondermann, 2011; Byrnes *et al.*, 2013; Morin-Leisk *et al.*, 2011). D-ATL has a glycine at the same position, and replacing it with cysteine to generate G343C D-ATL did not at all impair fusion activity (Supplemental Figure S4). As anticipated (Morin-Leisk *et al.*, 2011), cross-linked D-ATL soluble-domain dimers were captured in the presence of GMPPNP and also with GTP (albeit less so), but not with either GDP or in the absence of nucleotide (Figure 6A). Presumably, a lower level of cross-over dimers were captured after incubation with GTP, because the dimers form rapidly ($t_{1/2}$ ~ 1 s) but also undergo disassembly upon GTP consumption (Byrnes *et al.*, 2013), rendering them harder to capture in the subsequent cross-linking step. A higher percentage of cross-over dimer capture was seen with D-ATL (~66%) than was previously seen with ATL2 (~32%), possibly because the D-ATL cross-over dimer is more stable than its ATL2 counterpart. Finally, cross-over dimers were also captured efficiently with GDP-AlF_4^-. This was anticipated, based on the idea that cross-over is catalyzed by GTP hydrolysis, as well as the observation that ATL1 crystals formed with the transition-state analogue produced the cross-over dimer configuration (Byrnes *et al.*, 2013).

We next tested the ability of the salt bridge variant K320E D-ATL (with G343C) to undergo cross-over. As anticipated (Morin-Leisk *et al.*, 2011), GMPPNP-dependent cross-linking was inhibited for

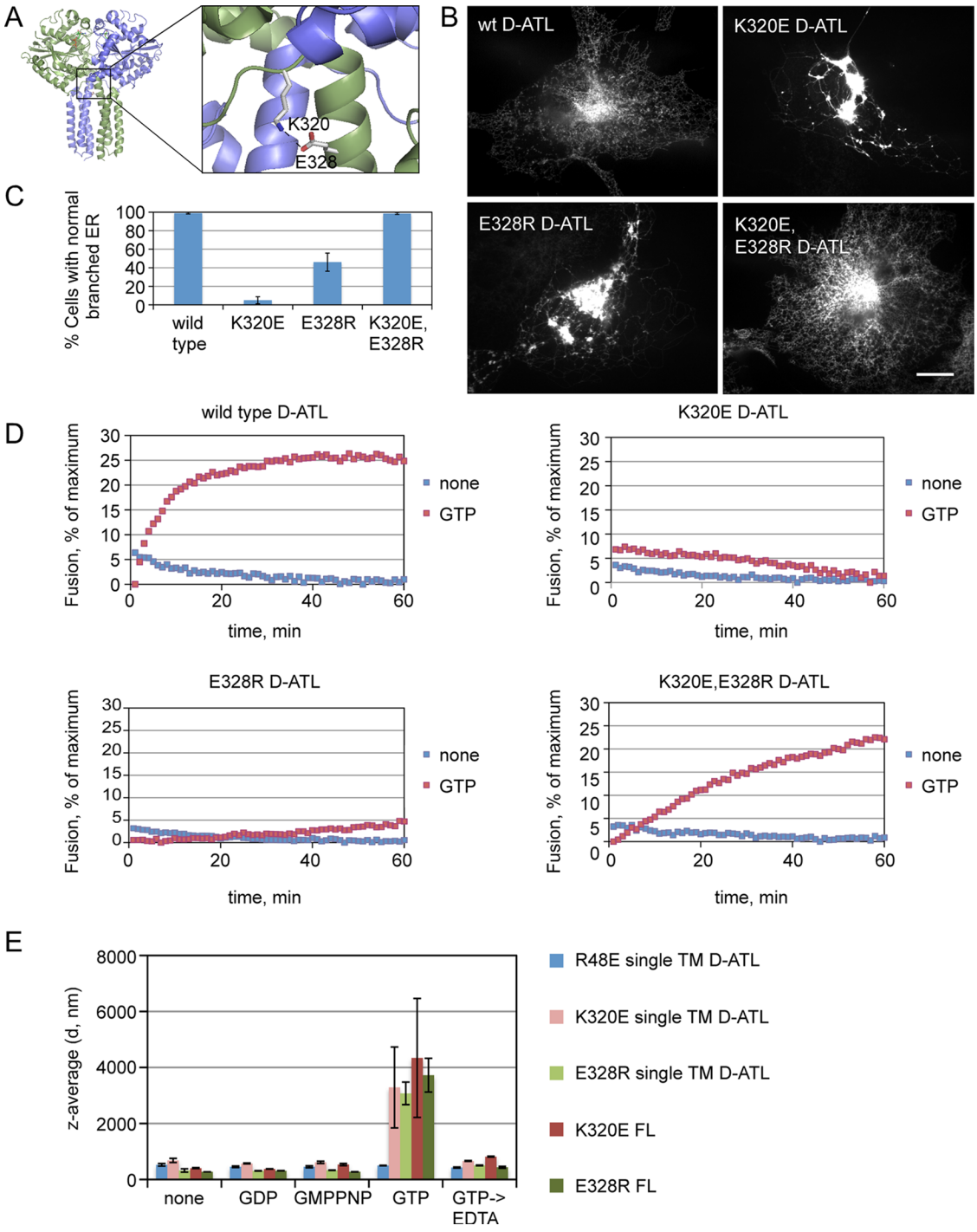

FIGURE 5: Fusion but not tethering depends on a K320-E328 salt bridge. (A) The position of the K320E-E328 salt bridge is superimposed onto a PyMOL rendering of the ATL1 cross-over dimer PDB 3QNU. (B) Expression of the individual K320E and E328R FL D-ATL variants but not the compensatory double-mutant (K320E,E328R) variant leads to abnormal ER network structure in Cos-7 cells. Cells transfected with the indicated eYFP-tagged variants were imaged 48 h later by confocal microscopy. Scale bar: 10 μm. (C) Quantification of the percent of expressing cells displaying a normal branched ER, >100 cells per measurement, average of three independent measurements ± SD. (D) The K320-E328 salt bridge is required for fusion. Wild-type, K320E, E328R, or the double-mutant (K320E,E328R) variant of FL D-ATL were reconstituted into donor and acceptor vesicles. Fusion was monitored by the dequenching of NBD-labeled lipid present in the donor vesicles in the presence or absence of GTP. (E) The K320-E328 salt bridge is not required for tethering. Either single TM or FL versions of either K320E or E328R D-ATL were incorporated into vesicles and incubated at 37°C for 5 min with the indicated nucleotides. Thereafter samples were subjected to DLS. For comparison, tethering by the single TM R48E D-ATL variant is also shown. The average of three independent measurements ± SD is shown for each condition.

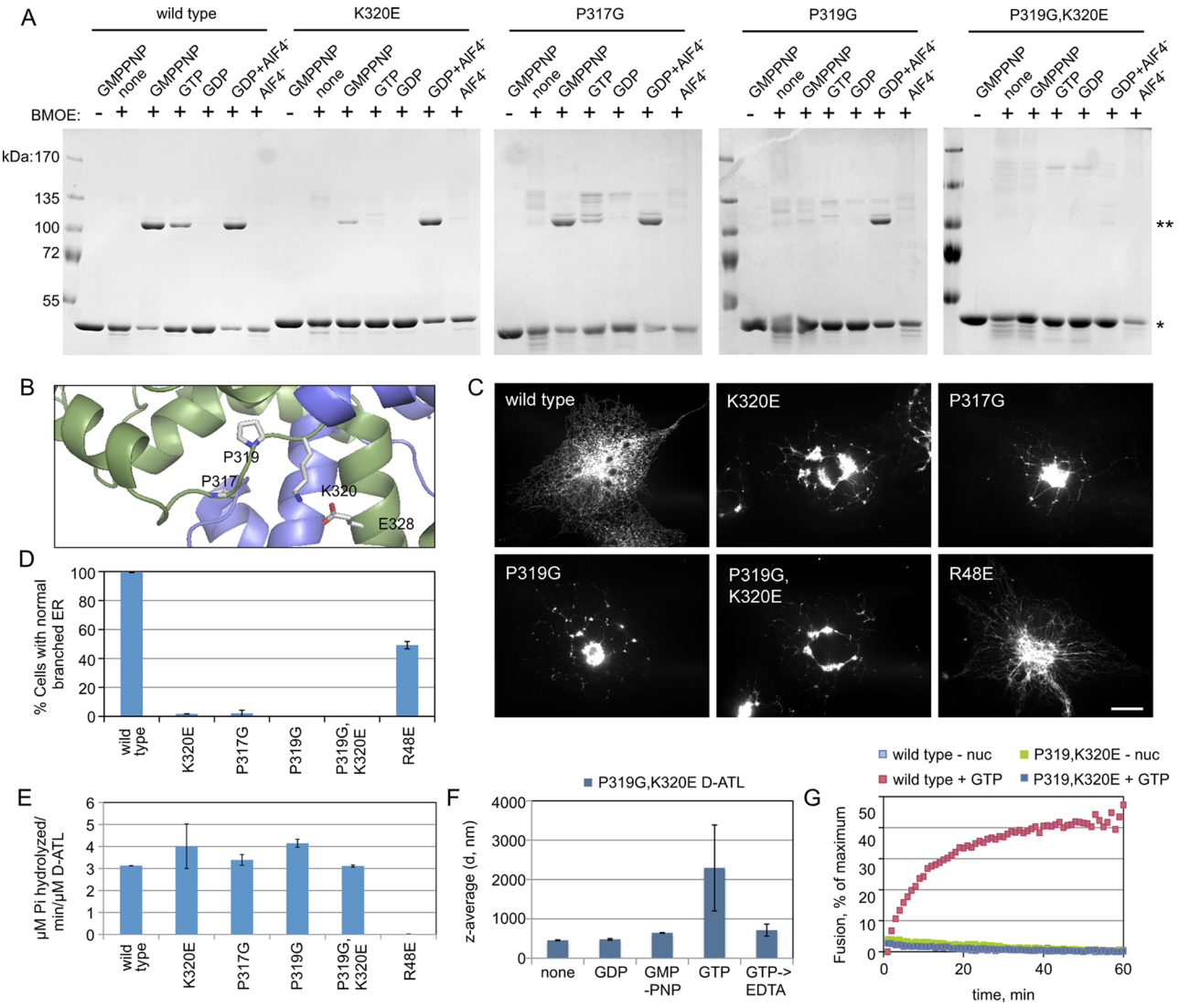

FIGURE 6: Tethering does not require cross-over. (A) The K320E mutation partially inhibits cross-over, but the double mutation P319G K320E abolishes it. The soluble domain of wild-type, K320E, P317G, P319G, or P319G K320E D-ATL was incubated at RT for 20 min in the presence or absence of the indicated nucleotides and then subjected to BMOE cross-linking. The single asterisk marks the soluble-domain monomer and the double asterisk marks the cross-linked dimer. All variants had the G343C substitution. (B) The positions of linker mutations made to block D-ATL cross-over superimposed onto a PyMOL rendering of the ATL1 cross-over dimer PDB 3QNU. (C) Expression of linker mutant variants in Cos-7 cells perturbs ER network morphology. Cells transfected with the indicated FL eYFP-tagged D-ATL mutant variants were visualized 48 h later by confocal microscopy. Scale bar: 10 µm. (D) The percent of cells expressing each variant and showing a normal branched ER, >100 cells per measurement, average of three independent measurements ± SD are quantified. The dimerization- and hydrolysis-defective R48E D-ATL is also shown for comparison. (E) Mutations that block cross-over do not impair GTPase activity. The soluble domain of each cross-over–defective variant was assayed for GTPase activity. The average of three independent measurements ± SD is shown. R48E is shown for comparison. (F) Cross-over–defective P319G K320E D-ATL can tether. Vesicles containing P319G K320E FL D-ATL were assessed for tethering by DLS after incubation at 37°C for 10 min in the presence or absence of the indicated nucleotides. The average of three independent measurements ± SD is shown for each condition. (G) The P319G K320E mutations block fusion. Wild-type or P319G K320E D-ATL was reconstituted into donor and acceptor vesicles. Fusion was monitored by the dequenching of NBD-labeled lipid present in the donor vesicles in the presence or absence of GTP.

this variant. But to our surprise, GDP-AlF_4^-–dependent cross-linking was not (Figure 6A). GDP-AlF_4^- was not tested in our previous analysis (Morin-Leisk *et al.*, 2011); therefore it remains to be clarified whether the same lack of sensitivity would also be observed for ATL2. Regardless, it was clear that the K320E mutation may impair but does not altogether block D-ATL cross-over.

Identifying new D-ATL mutations that abolish cross-over

The ability of the K320E variant to undergo cross-over, albeit reduced, raised an obvious concern that this variant retained activity in the tethering assay (Figure 5E), not because of a lack of requirement for cross-over in tethering, but because the K320E mutation only partially impaired cross-over. To address this concern, we

searched for a second mutation in a nearby residue that might eliminate cross-over altogether. Two proline residues in the linker connecting the 3HB to the GTPase head (P317 and P319) at or near the pivot point of the 3HB rotation (Figure 6B) seemed good candidates for mediating this rotation (Bian *et al.*, 2011; Byrnes and Sondermann, 2011). When expressed in Cos-7 cells, both P317G and P319G D-ATL variants, like the K320E variant, perturbed the ER network, indicating a loss of ER network–forming functionality (Figure 6C, quantified in 6D). As before, ER targeting was confirmed by counterstaining for cotransfected REEP5 (Supplemental Figure S3). In the cross-linking assay, the P317G mutation only slightly affected cross-over, whereas the P319G mutation had an inhibitory effect on par with the K320E mutation, inhibiting GMPPNP-dependent but not GDP-AlF_4^-–dependent cross-over (Figure 6A). Encouraged by the partial inhibition of cross-over caused by the P319G mutation, we tested whether it might result in a more potent block when combined with the K320E mutation. As expected, the double-mutant P319G K320E variant in Cos-7 cells also perturbed ER network morphology (Figure 6C, quantified in 6D). Strikingly, and in contrast to the single-mutant variants, the double-mutant variant displayed a complete block in our cross-linking assay, even in the presence of GDP-AlF_4^- (Figure 6A). The cross-linking assay was also attempted on membrane-anchored molecules, but technical issues hindered the analysis. Still, given the complete block exhibited by the double-mutant soluble domain, it was difficult to envision any cross-over capability on the part of the more constrained membrane-anchored counterpart. In sum, the combined P319G K320E mutations were likely to provide an effective means of blocking cross-over.

One final concern was that the double P319G K320E mutations might not only block cross-over but also impair GTP hydrolysis. Recent work had revealed a sensitivity of GTP loading to mutations in 3HB residues outside the GTPase domain, presumably because the mutations impeded packing of the 3HB against the α6 helix within the head (Byrnes *et al.*, 2013). Therefore it was imperative that any effect of the P319G K320E mutation on GTP loading or GTP hydrolysis be ruled out. GTPase assays revealed that all variants, including P319G K320E, were as active as the wild-type protein in their ability to hydrolyze GTP, confirming that the mutations selectively impaired cross-over (Figure 6E).

Tethering does not depend on cross-over

Finally, we tested for the ability of the hydrolysis-active, but cross-over–defective, P319G K320E variant to mediate tethering. As with either the single TM or FL versions of the K320E variant (Figure 5E), the double-mutant P319G K320E FL variant still tethered membranes robustly and in a manner dependent on hydrolyzable GTP (Figure 6F). As also seen for the K320E FL variant, the P319G K320E FL variant lacked any detectable fusion activity (Figure 6G). On the basis of the lack of impairment of tethering by either the K320E or P319G K320E mutations, we were compelled to conclude that membrane tethering by D-ATL depends strictly on GTP hydrolysis but not on forming the cross-over configuration. Importantly, tethering by either the K320E or P319,K320E mutant variants, both of which retained the second TM helix and tail, was morphologically similar to that seen with single TM D-ATL, with zipper-like parallel-aligned membrane interfaces (Figure 3C) that were seen more frequently with GTP than without (Figure 3D). In addition, although further structural work will be required to fully resolve the difference, "zippers" formed with the cross-over–defective P319G K320E variant appeared slightly wider than those formed with either the partially cross-over–defective (K320E) or cross-over–competent (single TM) variants, suggestive of a more extended tether in the absence of cross-over (Figure 3D).

DISCUSSION

GTP hydrolysis catalyzes stable *trans* pairing for tethering

We observed *trans* pairing between opposing membrane-anchored D-ATL, as defined by vesicle tethering, to be GTP dependent under a variety of conditions: either when D-ATL was anchored by a single TM helix (Figure 4), two TM helices (Figures 4 and 5E), or both TM helices and the C-terminal tail (Figures 5E and 6F). Furthermore, under no condition did the nonhydrolyzable analogue GMPPNP (or GTPγS, Supplemental Figure S2) substitute for GTP. Also consistent with a requirement for hydrolyzable GTP, the R48A variant, defective specifically for nucleotide hydrolysis (Pendin *et al.*, 2011; Byrnes *et al.*, 2013), failed to tether (Figure 4).

The implication that nucleotide hydrolysis might be a prerequisite for, rather than a consequence of, stable *trans* pairing may seem counterintuitive, especially because stable truncated ATL dimers were readily captured with the nonhydrolyzable GTP analogue GMPPNP (Byrnes and Sondermann, 2011; Morin-Leisk *et al.*, 2011; also Figure 6A). However, given the recent observation that dimer formation and cross-over were both 100-fold faster with hydrolysis than without (Byrnes *et al.*, 2013), it is now evident that the ready accumulation of truncated stable dimers in the absence of hydrolysis was likely a reflection of the stability of the cross-over dimer configuration rather than a reflection of the GTP-bound state triggering cross-over. Indeed, the form 1 cross-over dimer was initially crystallized in the presence of GDP (Bian *et al.*, 2011), which generally fails to induce dimer formation in solution (Byrnes and Sondermann, 2011; Morin-Leisk *et al.*, 2011; Moss *et al.*, 2011). Thus the physiological trigger for stable dimer formation is likely not the binding but rather the hydrolysis of GTP. As alluded to in the *Results* section, we speculate that hydrolysis may be triggered by an initial low-affinity *trans* interaction between GTP-bound heads, which may stimulate hydrolysis in a GAP-like manner through rearrangement of an arginine finger within each head, with hydrolysis in turn generating the high-affinity head-to-head contacts necessary for a productive fusion event.

Collectively our findings are most consistent with the role of GTP hydrolysis in the model put forth recently by Sondermann and colleagues, in which GTP hydrolysis triggers the formation of head contacts required to tether opposing membranes in preparation for fusion (Byrnes *et al.*, 2013). This aspect of their model, based solely on conformational analysis of the ATL1 soluble domain, is now well supported for membrane-anchored D-ATL in the context of the fusion reaction. However, in contrast to another aspect of their model, in which cross-over serves primarily to tether opposing membranes in *trans* (Byrnes *et al.*, 2013), our findings indicate that cross-over is dispensable for tethering in the context of the fusion reaction.

Cross-over formation is not required to tether membranes

We concluded that *trans* pairing is independent of cross-over configuration formation, because robust tethering was observed by D-ATL variants that were essentially cross-over defective (Figure 6, A and F). Two potential caveats to this interpretation are worth consideration, however. First, because our assay for cross-over competency is a soluble-phase assay, there is a possibility that the membrane-anchored P319G K320E variant is able to achieve the cross-over configuration, even though the truncated molecule cannot. We consider this possibility unlikely, because membrane anchoring would be more likely to impede rather than promote cross-over. The absence of any detectable cross-linked product, even under the relatively permissive conditions of our soluble-phase assay, which captures both slow and fast cross-over events (Byrnes *et al.*, 2013), likely reflects complete or near-complete loss of cross-over capability on the

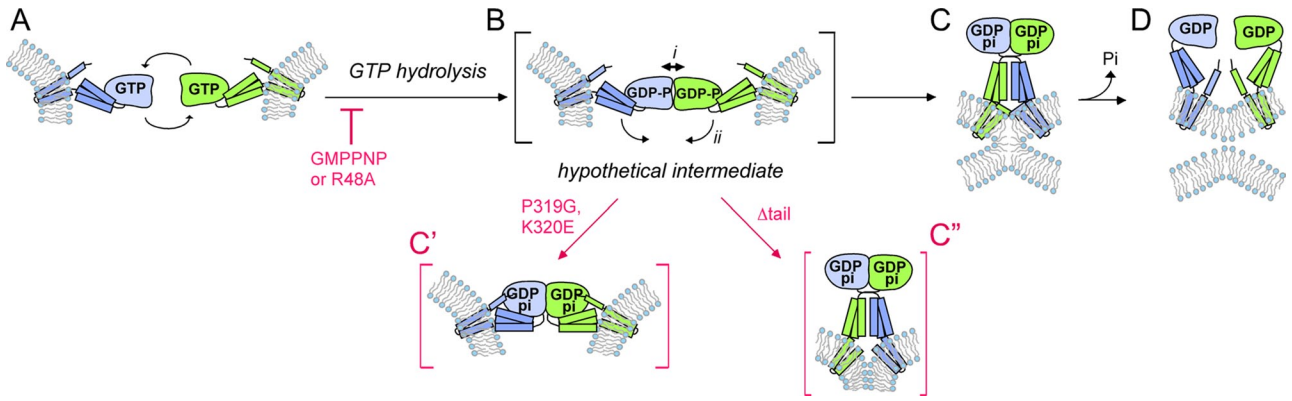

FIGURE 7: Working model for D-ATL–catalyzed membrane tethering and fusion. (A) GAP-like intermolecular interactions between GTP-bound subunits on opposing membranes triggers GTP hydrolysis. (B) Hydrolysis initiates conformational changes in the GTPase head (a short-lived hypothetical intermediate is shown in brackets) to simultaneously stabilize head-to-head contact for stable *trans* pairing (i) and release the 3HB for cross-over (ii). Stable *trans* pairing tethers opposing membranes to one another, while cross-over, with assistance from the tail, powers fusion (C). After fusion, P_i release may trigger dimer disassembly for subunit recycling (D). Both tethering and fusion are inhibited when hydrolysis is blocked by either GMPPNP or the catalytic R48A mutation. C′ and C″ depict tethered intermediates (bracketed in red) that accumulate either when cross-over is blocked by P319G K320E mutation (C′) or when the absence of the tail permits cross-over but not lipid mixing (C″).

part of the P319G K320E variant. A second caveat pertains to the definition of cross-over. Dimer capture with BMOE, with its 8-Å spacer arm, is expected to depend on close parallel 3HB alignment. A hybrid conformation, with the 3HBs neither fully extended nor fully parallel aligned, could form and yet escape capture by BMOE cross-linking. Therefore our conclusions are necessarily limited to assessing the requirement for the fully parallel-aligned cross-over conformation. Regardless, our results provide compelling evidence that the ability of D-ATL to undergo full cross-over is not a prerequisite for tethering.

Cross-over formation may power lipid mixing

Even though full cross-over formation was not essential to tethering, it is likely necessary for membrane fusion. The K320E D-ATL variant, only partially defective for cross-over (Figure 6A), was nevertheless fusion incompetent (Figure 5D; Bian *et al.*, 2011). Similarly, the P317G and P319G mutations each only mildly or partially impairing cross-over (Figure 6A), respectively, exerted dominant-negative effects on ER morphology consistent with a fusion defect (Figure 6, C and D). These observations suggest that membrane fusion may require formation of most or all of the contacts observed in the form 3 conformer, with loss of even a subset of stabilizing contacts impairing fusion activity. We speculate that the binding energy of cross-over therefore contributes substantially to catalyzing lipid mixing for fusion.

A working model for ATL-catalyzed fusion

On the basis of the information at hand, we suggest the following working model for the ATL fusion reaction cycle (Figure 7). The model starts with ATL molecules on opposing membranes encountering one another in the GTP-bound state (Figure 7A), followed by GAP-like interactions between heads in *trans*. Because tethering was not observed with nonhydrolyzable GTP or with the R48A hydrolysis-defective variant, we speculate that these GAP-like interactions are weak head contacts that nevertheless are sufficient to induce rearrangement of catalytic residues required for hydrolysis (Figure 7B). We suggest that GTP hydrolysis in turn catalyzes conformational changes within the head that 1) strengthen the initial head contact, resulting in a stably engaged *trans* dimer for tethering; and 2) simultaneously release the 3HBs from the heads to enable cross-over for fusion (Figure 7C). Though our results are also compatible with tethering occurring upstream of cross-over formation, the concerted tethering and cross-over depicted in the model are more consistent with the recent observation that head contact and cross-over are both triggered near simultaneously in the soluble phase (Byrnes *et al.*, 2013). Once fusion has occurred, we further speculate that P_i release induces disassembly of the cross-over dimer for subunit recycling (Figure 7D). Many of the details of our working model remain to be clarified, particularly with regard to the upstream *trans* interactions that lead to hydrolysis and the downstream steps that drive dimer disassembly. Yet the model provides a framework that is largely consistent with observations made within this study and previous observations by others. For instance, inhibition of nucleotide hydrolysis blocks the reaction cycle before tether formation (Figure 4). In contrast, inhibition of cross-over formation does not impede tether formation, though it does block fusion (Figure 6, F and G). Finally, truncation of the molecule to remove the lipid-destabilizing effects of the tail blocks fusion (Moss *et al.*, 2011; Liu *et al.*, 2012) but still enables tethering (Figures 1 and 2). In the latter two cases, the putative tethered intermediates that accumulate as a consequence of mutation have been visualized directly by cryo-EM (Figure 3). In the case of the single TM variant lacking the tail, the tethered bilayers were tightly opposed, as would be predicted by stable *trans* interaction involving cross-over. Remarkably, the presumptive tethered membrane interfaces formed without cross-over (P319G K320E) were slightly wider, corresponding to a somewhat longer distance between inner leaflet densities. This would be consistent with the formation of a more extended tether in the absence of cross-over formation. However, further analysis will be required to fully resolve these structural differences.

In summary, our findings provide new insights into the conformational coupling of membrane-bound ATL to its GTP hydrolysis cycle and begin to reveal the role of the cross-over conformation change in the fusion mechanism. Future work should enable continued refinement of our understanding of how the ATL mechanochemical cycle powers the fusion of ER membranes.

MATERIALS AND METHODS

Cells, constructs, and reagents

Cell expression studies were conducted on Cos-7 cells maintained at 37°C in a 5% CO_2 incubator in DMEM (Sigma-Aldrich, St. Louis, MO) and 10% fetal bovine serum (Atlanta Biologicals, Atlanta, GA) with 1% penicillin/streptomycin (Thermo Fisher Scientific, Waltham, MA). N-terminally enhanced yellow fluorescent protein (eYFP)-tagged D-ATL was kindly provided by James McNew (Rice University, Houston, TX). The 6×His-tagged D-ATL was constructed for protein production using PCR amplification of nucleotides encoding amino acids 1–541 of D-ATL from eYFP-D-ATL and cloned into the pRSETB vector at *Nhe*I and *Eco*RI sites. Mutations specific to this study were generated using QuikChange mutagenesis (Qiagen, Valencia, CA) and fully verified by sequencing (Genewiz, South Plainfield, NJ). With the exception of Figure 6, all variants used for protein production in this study, including the wild-type, had the following additional amino acid changes: G343C, C350A, C429L, C452L, and C501A. These substitutions were introduced at the outset for the express purpose of restricting the reactivity of the sulfhydryl-reactive cross-linker BMOE (Thermo Fisher Scientific, Plainfield, NJ) to the G343 position. Notably, a D-ATL version containing all of the indicated substitutions had fusion activity similar to that of the unaltered D-ATL (Supplemental Figure S4). The variants used in Figure 6 had none of the above cysteine substitutions. The Myc-REEP5 construct was previously described (Morin-Leisk *et al.*, 2011). All lipids were purchased from Avanti Polar Lipids (Alabaster, AL). GTP, GDP, GMPPNP, and GTPγS were purchased (Sigma-Aldrich), reconstituted to 100 mM stocks in 10 mM Tris, 1 mM EDTA (pH 8.0), and stored at –80°C.

Protein expression and purification

Protein expression was induced with 0.2 mM isopropyl β-D-1-thiogalactopyranoside in BL21(DE3)pLysS cells at 16°C for 2.5 h. Cells were lysed in 4% Triton X-100 (Roche, Basel, Switzerland) in a standard lysis buffer, and 6×His-tagged proteins were purified using standard protocols on Ni^{+2} agarose beads (Qiagen). Bound protein was eluted in 50 mM Tris (pH 8.0), 250 mM imidazole, 100 mM NaCl, 5 mM $MgCl_2$, 10% glycerol, 2 mM 2-mercaptoethanol, 0.1% Anapoe-X 100 (Affymetrix, Santa Clara, CA), and 1 mM EDTA. Protein yields were typically 4–8 mg/ml (~1 mg per liter of culture), > 85% pure, flash frozen in liquid N_2, and stored at –80°C.

Proteoliposome production

Lipids in chloroform dried down by rotary evaporation were hydrated by resuspension in A100 buffer (25 mM HEPES, pH 7.4, 100 mM KCl, 10% glycerol, 2 mM β-mercaptoethanol, 1 mM EDTA; Moss *et al.*, 2011), final lipid concentration ~10 mM, and subjected to 12 freeze–thaw cycles in liquid N_2 and room temperature (RT) water. Liposomes (100- to 300-nm diameter) were formed by extrusion through 100-nm polycarbonate filters using the LipoFast LF-50 extruder (Avestin, Ottawa, ON, Canada) and checked for size by DLS (as described below and in Supplemental Figure S1). Unlabeled liposomes consisted of 1-palmitoyl-2-oleoyl-*sn*-glycero-3-phosphocholine:1,2-dioleoyl-*sn*-glycero-3-phospho-L-serine (85:15), and labeled liposomes had 1-palmitoyl-2-oleoyl-*sn*-glycero-3-phosphocholine:1,2-dioleoyl-*sn*-glycero-3-phospho-L-serine:1,3-dipalmitoyl-*sn*-glycero-3-phosphoethanolamine-*N*-(7-nitro-2-1,3-benzoxadiazol-4-yl:1,2-dipalmitoyl-*sn*-glycero-3-phosphoethanolamine-*N*-(lissamine rhodamine B sulfonyl) (82:15: 1.5:1.5). D-ATL in 0.1% Anapoe-X 100 was reconstituted into preformed 100-nm liposomes as previously described (Orso *et al.*, 2009; Moss *et al.*, 2011). In brief, all reconstitutions were carried out at a protein-to-lipid ratio of 1:300 at an effective detergent-to-lipid ratio of ~0.7, as previously described (Moss *et al.*, 2011). Protein and lipid were incubated at 4°C for 1 h. Detergent was removed by SM-2 Bio-Beads (Bio-Rad, Hercules, CA) at 70 mg Anapoe X-100 per 1 g of beads. Insoluble protein aggregates were pelleted by centrifugation of the samples in a microcentrifuge for 10 min at 16,000 × *g*. Thereafter reconstituted D-ATL proteoliposomes were adjusted to 50% Nycodenz and separated from unincorporated protein by flotation of proteoliposomes through a (50%/45%/0%) Nycodenz (Axis-Shield, Dundee, Scotland) 5-ml step gradient. All Nycodenz solutions were made in A100 buffer without glycerol. After centrifugation at 40,000 rpm for 16 h at 4°C in a SW-50.1 rotor, the gradient was fractionated and analyzed by SDS–PAGE stained with Coomassie blue to assess insertion efficiency. The proteoliposomes typically migrated to the 45%/0% Nycodenz interface. Finally, the floated fraction was desalted over a 2.4-ml Sephadex A (GE Healthcare) column into A100 buffer, stored at 4°C, and used within 72 h.

Fusion assay

Fusion assays were performed as previously described (Moss *et al.*, 2011), except that donor and acceptor proteoliposomes were mixed at a molar ratio of 1:2. In brief, labeled donor proteoliposomes (0.2 mM) were mixed with unlabeled acceptor proteoliposomes (0.4 mM) in A100 buffer in the presence of 5 mM $MgCl_2$ in a total volume of 200 µl per reaction. The reaction mixture was transferred into a clear, flat-bottomed polystyrene 96-well plate (Corning, Corning, NY) and incubated at 37°C for 10 min. The fusion reaction was started by addition either of 2 mM GTP, 2 mM GMPPNP (final concentration), or buffer. NBD fluorescence (excitation: 460 nm; emission: 538 nm) was measured at 1-min intervals with a 1-s shaking after every read. After 60 min, 10 µl of 10% Anapoe X-100 was added to determine the total fluorescence in the sample. All measurements, reported as the percent of total fluorescence after solubilization in Anope X-100, were acquired on a Tecan Safire II fluorescence plate reader (Tecan, Mannedorf, Switzerland) using Microsoft Excel (Microsoft, Redmond, WA).

DLS

Proteoliposomes (1 mM total lipid) in A100 buffer were incubated in the absence or presence of 2 mM GTP, GDP, or GMPPNP, all in the presence of 5 mM $MgCl_2$. Incubations were for 10 min at 37°C unless indicated otherwise. Only for P319G K320E D-ATL, the $MgCl_2$ concentration was lowered to 3 mM to reduce a low level of size shift seen in the absence of nucleotide. Thereafter the reaction was diluted 10-fold (0.1 mM total lipid) into A100 buffer + 5 mM $MgCl_2$ in a disposable polystyrene cuvette (Thermo Fisher Scientific). Measurements were acquired on a Malvern ZetaSizer Nano Series (model Zen3600; Malvern, UK) instrument. Parameters were set automatically by the instrument software (Dispersion Technology Software, version 5). Where indicated, EDTA was added to samples after the initial measurement to a final concentration of 40 mM, and the measurements were repeated after 10 min. The average of three measurements per sample was used to represent the *z*-average of the vesicles.

Cryo-EM

Proteoliposomes in A100 buffer + 5 mM $MgCl_2$ were incubated in the absence or presence of 2 mM GTP for 20 min at RT. Reaction solutions (4 µl) were applied onto R 2/1 Quantifoil R2/1 holey carbon EM grids (Quantifoil Micro Tools, Jena, Germany), blotted from the back side of the grid for 3–4 s, and manually plunged frozen into liquid ethane. The frozen grids were loaded onto a Gatan 626

single-tilt liquid N_2 cryo-holder (Gatan, Warrendale, PA) and imaged at 200 kV with an FEI TF20 microscope (FEI, OR). Low-dose (~20 electron/Å^2) projection images were recorded on a 4k × 4k UltraScan 4000 CCD camera (Gatan) under focus of ~2 µm and nominal magnifications of 50,000×. A total of 70–100 images were recorded from randomly selected areas in each cryo-specimen. The width of the zipper-like structures was determined by measuring the distance between the two outer dark-density peaks from opposing membranes using the line profile function in the Digital Micrograph software (Gatan). Only the images recorded under similar defocus values were used for the analysis. The average width was calculated from 10–15 straight "zipper" profiles.

Fluorescence microscopy

Cos-7 cells on 12-mm glass coverslips (24-well plate) were transfected with 100 ng of the indicated eYFP-D-ATL plasmids and 1.5 µl Lipofectamine 2000 transfection reagent (Life Technologies, Grand Island, NY) according to the manufacturer's instructions. At 48 h following transfection, cells were fixed in 3% paraformaldehyde in phosphate-buffered saline, washed, and mounted directly. For REEP5 colocalization, cells were cotransfected with 50-ng eYFP-D-ATL and 50-ng Myc-REEP5, fixed in ice-cold MeOH, and stained as previously described (Morin-Leisk *et al.*, 2011) with the 9E10 monoclonal antibody against the Myc epitope followed by Alexa Fluor 568–conjugated goat anti-mouse secondary antibody (Life Technologies). Images were obtained using a spinning-disk confocal scanhead (Yokagawa; PerkinElmer, Akron, OH) mounted on an Axiovert 200 microscope (Zeiss, Thornwood, NY) with a 100× 1.4 NA objective (Zeiss) and acquired using a 12-bit ORCA-ER camera (Hamamatsu Photonics, Hamamatsu City, Japan). Maximal value projections of sections at 0.2-µm spacing were acquired using Micro-manager open-source software (University of California, San Francisco, San Francisco, CA).

Cross-linking

Purified 6×His-tagged D-ATL (residues 1–415) and variant proteins were dialyzed into SEC buffer (25 mM Tris-HCl, pH 7.0, 100 mM NaCl, 5 mM $MgCl_2$, 2 mM EGTA) at 4°C and precleared by centrifugation at 100,000 rpm for 15 min (TLA100). A 5 µM sample of each protein was incubated at RT in SEC buffer (pH 7.0) in the absence or presence of 2 mM GMPPNP, GDP, GTP, GDP-AlF_4^- (2 mM GDP/2 mM $AlCl_3$/20 mM NaF), or AlF_4^- only (2 mM $AlCl_3$/20 mM NaF). After 30 min at RT, the reaction was diluted 2.5-fold into SEC (to 2 µM D-ATL) in the absence or presence of 6 µM BMOE (Thermo Fisher Scientific) and incubated for 1 h at RT. Samples were then quenched with 20 mM dithiothreitol for 15 min, mixed with reducing sample buffer, resolved by SDS–PAGE, and stained with Coomassie blue.

GTPase assay

Purified 6×His-tagged D-ATL (residues 1–415) and variant proteins were dialyzed into 50 mM Tris-HCl (pH 7.5), 100 mM NaCl, 1 mM $MgCl_2$ at 4°C, and precleared by centrifugation at 100,000 rpm (TLA100) at 4°C for 15 min. GTPase activity was measured using the Enzchek Phosphate Assay kit (Life Technologies). A standard reaction for GTPase measurements involved mixing 1 U/ml purine nucleoside phosphorylase (PNP), 0.2 mM 2-amino-6-mercapto-7-methylpurine riboside (MESG) in the provided buffer (50 mM Tris-HCl, pH 7.5, 1 mM $MgCl_2$, 0.1 mM sodium azide) supplemented with 100 mM NaCl and 0.5 mM GTP in a total volume of 200 µl. After 10 min at 37°C, reactions were transferred to a 96-well plate (Corning) and started by addition of either buffer or 6×His-tagged D-ATL variants at a final concentration of 1 or 2 µM. Absorbance at 360 nm was monitored at 30-s intervals for 30 min at 37°C in a plate reader (Tecan, Safire 2). Data were normalized to a phosphate standard, and initial velocities were calculated using the early linear portion of each curve.

ACKNOWLEDGMENTS

James McNew (Rice University, Houston, TX) kindly provided the eYFP-D-ATL construct and also provided helpful advice on the fusion assay. The Molecular Biosensor Imaging Facility, B. Armitage, and J. Minden (Carnegie Mellon University, Pittsburgh, PA) shared instruments necessary for this study. A. Linstedt gave helpful comments on the manuscript, and members of the Lee, Linstedt, and Puthenveedu labs offered helpful comments throughout. This work was funded by grants from the National Institutes of Health (NIH; 1R21DK088208 and R01GM107285) and the Spastic Paraplegia Foundation to T.H.L. and a grant from the NIH (GM085043) to P.Z.

REFERENCES

Allan VJ, Vale RD (1991). Cell cycle control of microtubule-based membrane transport and tubule formation in vitro. J Cell Biol 113, 346–359.

Anwar K, Klemm RW, Condon A, Severin KN, Zhang M, Ghirlando R, Hu J, Rapoport TA, Prinz WA (2012). The dynamin-like GTPase Sey1p mediates homotypic ER fusion in *S. cerevisiae*. J Cell Biol 197, 209–217.

Arac D, Chen X, Khant HA, Ubach J, Ludtke SJ, Kikkawa M, Johnson AE, Chiu W, Sudhof TC, Rizo J (2006). Close membrane-membrane proximity induced by Ca^{2+}-dependent multivalent binding of synaptotagmin-1 to phospholipids. Nat Struct Mol Biol 13, 209–217.

Bian X, Klemm RW, Liu TY, Zhang M, Sun S, Sui X, Liu X, Rapoport TA, Hu J (2011). Structures of the atlastin GTPase provide insight into homotypic fusion of endoplasmic reticulum membranes. Proc Natl Acad Sci USA 108, 3976–3981.

Byrnes LJ, Singh A, Szeto K, Benvin NM, O'Donnell JP, Zipfel WR, Sondermann H (2013). Structural basis for conformational switching and GTP loading of the large G protein atlastin. EMBO J 32, 369–384.

Byrnes LJ, Sondermann H (2011). Structural basis for the nucleotide-dependent dimerization of the large G protein atlastin-1/SPG3A. Proc Natl Acad Sci USA 108, 2216–2221.

Friedman JR, Webster BM, Mastronarde DN, Verhey KJ, Voeltz GK (2010). ER sliding dynamics and ER-mitochondrial contacts occur on acetylated microtubules. J Cell Biol 190, 363–375.

Ghosh A, Praefcke GJ, Renault L, Wittinghofer A, Herrmann C (2006). How guanylate-binding proteins achieve assembly-stimulated processive cleavage of GTP to GMP. Nature 440, 101–104.

Hashimoto Y, Shirane M, Matsuzaki F, Saita S, Ohnishi T, Nakayama KI (2014). Protrudin regulates endoplasmic reticulum morphology and function associated with the pathogenesis of hereditary spastic paraplegia. J Biol Chem 289, 12946–12961.

Lee C, Chen LB (1988). Dynamic behavior of endoplasmic reticulum in living cells. Cell 54, 37–46.

Lee C, Ferguson M, Chen LB (1989). Construction of the endoplasmic reticulum. J Cell Biol 109, 2045–2055.

Liu TY, Bian X, Sun S, Hu X, Klemm RW, Prinz WA, Rapoport TA, Hu J (2012). Lipid interaction of the C terminus and association of the transmembrane segments facilitate atlastin-mediated homotypic endoplasmic reticulum fusion. Proc Natl Acad Sci USA 109, E2146–E2154.

McNew JA, Sondermann H, Lee T, Stern M, Brandizzi F (2013). GTP-dependent membrane fusion. Annu Rev Cell Dev Biol 29, 529–550.

Morin-Leisk J, Saini SG, Meng X, Makhov AM, Zhang P, Lee TH (2011). An intramolecular salt bridge drives the soluble domain of GTP-bound atlastin into the postfusion conformation. J Cell Biol 195, 605–615.

Moss TJ, Andreazza C, Verma A, Daga A, McNew JA (2011). Membrane fusion by the GTPase atlastin requires a conserved C-terminal cytoplasmic tail and dimerization through the middle domain. Proc Natl Acad Sci USA 108, 11133–11138.

Orso G, Pendin D, Liu S, Tosetto J, Moss TJ, Faust JE, Micaroni M, Egorova A, Martinuzzi A, McNew JA, *et al*. (2009). Homotypic fusion of ER membranes requires the dynamin-like GTPase atlastin. Nature 460, 978–983.

Park SH, Blackstone C (2010). Further assembly required: construction and dynamics of the endoplasmic reticulum network. EMBO Rep 11, 515–521.

Pendin D, Tosetto J, Moss TJ, Andreazza C, Moro S, McNew JA, Daga A (2011). GTP-dependent packing of a three-helix bundle is required for atlastin-mediated fusion. Proc Natl Acad Sci USA 108, 16283–16288.

Shibata Y, Shemesh T, Prinz WA, Palazzo AF, Kozlov MM, Rapoport TA (2010). Mechanisms determining the morphology of the peripheral ER. Cell 143, 774–788.

Waterman-Storer CM, Salmon E (1998). Endoplasmic reticulum membrane tubules are distributed by microtubules in living cells using three distinct mechanisms. Curr Biol 8, 798–806.

Zhang M, Wu F, Shi J, Zhu Y, Zhu Z, Gong Q, Hu J (2013). ROOT HAIR DEFECTIVE3 family of dynamin-like GTPases mediates homotypic endoplasmic reticulum fusion and is essential for *Arabidopsis* development. Plant Physiol 163, 713–720.